JOURNAL OF GUIDANCE, CONTROL, AND DYNAMICS
Vol. 17, No. 4, July–August 1994

Sun-Tracking Commands and Reaction Wheel Sizing with Configuration Optimization

Hari B. Hablani*
Rockwell International, Space Systems Division, Seal Beach, California 90740

This paper is composed of two parts. In the first part, two-axis sun-tracking commands for solar arrays articulated to Earth-pointing spacecraft are developed. In the second, the paper deals with optimization of cant angle(s) of reaction wheel pyramids for minimizing power consumption and required torque and momentum capacity of the wheels to deliver a cylindrical momentum envelope and a rectangular parallelepiped torque envelope. The two commonly used four-wheel pyramid configurations and a new one, according to which the wheels are inclined to roll and yaw axes of the spacecraft at unequal angles, are analyzed in depth. The minimum torque and momentum capacity of each wheel in the four-wheel pyramids are compared with the capacity of each wheel in six- and three-wheel pyramids. Both no-wheel-failure and one-wheel-failure cases are considered for all pyramidal configurations. The literal relationships developed in the paper are very useful for quickly determining the optimum cant angle(s) and the torque and momentum capacity of the wheels for given requirements about the spacecraft axes, and for selecting a most suitable wheel configuration from six- and three-wheel pyramids, three four-wheel pyramids of different bases, and six- and three-wheel orthogonal arrangements.

I. Introduction

THIS paper has a two-fold objective: 1) determination of sun-tracking commands for solar array(s) attached to Earth-observing spacecraft, and 2) reaction wheel sizing and its pyramid configuration optimization for maximum momentum storage and minimum power consumption. These two apparently unconnected topics are linked through momentum accumulation, caused by solar radiation torque, over an orbit and its annual variation. Although the topics at hand are classical, it seems there is no reference in the literature that treats this subject sufficiently comprehensively. This paper is contemplated, therefore, to fulfill that need. The contents of the paper, with previous contributions in perspective, are as follows.

The spacecraft mission and orbit geometry influence the pointing commands for solar arrays and spacecraft attitude control system significantly. For an Earth-pointing, three-axis stabilized spacecraft rotating once per orbit about the orbit normal, an attached solar array should at least have one relative rotational degree of freedom about the orbit normal, so that it can be held inertially fixed and sun pointing. Geosynchronous (orbit inclination $i = 0$ deg) and sun-synchronous ($i > 90$ deg) spacecraft, each with one solar array at a *fixed* inclination angle (commonly known as β angle) with the orbit plane, are two examples. However, in neither example the sun remains normal to the solar array through all seasons because of a fixed β, the off normality being no more than $\pm\ \lambda$ ($\lambda = 23.44$ deg, the angle between the ecliptic and the equatorial planes) in the first example, and a narrower range in the second; the corresponding power loss, therefore, is always less than or equal to 8.25%, compensated for by oversizing the array proportionally. For a spacecraft in a general orbit, the β angle of the sun rays, due to nodal regression and the motion of the Earth around the sun, varies in the range $-(\lambda + i) \leq \beta \leq (\lambda + i)$ several times in a year. Clearly, as the orbit inclination increases, the range of β expands and if, for simplicity, the solar array is opted not to have a second rotational degree of freedom, the power loss arising from the off normality of the sun rays becomes significant. To minimize this power loss, some spacecraft are designed to rotate about the yaw axis by 180 deg once in a few months when the sun crosses the orbit plane. An additional significant benefit of this yaw rotation (in fact, a strong reason for it) is that a thermal radiator, placed on the opposite y face of the spacecraft, will then always see the cold side of the orbit, as desired for thermal radiation. With the 180 deg yaw rotations, the range of β is curtailed to $0 \leq \beta \leq (\lambda + i)$, and so the solar array is now fixed to the spacecraft at $(\lambda + i)/2$ deg with the orbit plane, resulting in a power loss of $1 - \cos[(\lambda + i)/2]$ at the most. For the spacecraft in high inclination (but less than 90 deg) orbits, this power loss may still be prohibitive, and so an alternative scheme may be adopted, according to which the spacecraft follows a continuous yaw command profile in order for the solar array to remain normal to the sun rays essentially all the time, resulting in no power loss. For example, Ocean Topography Experiment (TOPEX) ($i = 63.1$ deg) and Global Positioning System ($i = 60$ deg) spacecraft employ this scheme. McElvain[1] and Dennehy et al.[2] have presented the corresponding sun-tracking commands. These persistent yaw rotations, however, interfere with some Earth-observing missions (reconnaissance and surveillance, for example), and Kalweit[3] has determined the best-fit, minimum-power-loss, average yaw angles for them, constant over each half-orbit. Parenthetically, Kalweit[3] considers solar array rotation about the roll axis, instead of the more familiar pitch axis, because then the atmospheric disturbance torque about the yaw axis for low Earth orbits is virtually zero. Regardless, if even these half-orbit-apart yaw rotations are objectionable, the last alternative—imposing a complexity of some degree—is a solar array with two rotational degrees of freedom. It is this arrangement that is considered in Sec. II, wherein the corresponding sun-tracking commands about both axes are developed. The β commands are discussed and illustrated in view of the nodal regression and the Earth's motion around the sun. Solar radiation torque, attendant momentum accumulation over each orbit, and its annual variation are briefly summarized in Sec. III, providing an example of a cylindrical momentum envelope requirement for sizing reaction wheels. Of course, a momentum envelope, particularly for near Earth orbits, is governed by other environmental torques as well: aerodynamic, gravity gradient, or magnetic disturbances, possibly leading to elliptic envelopes oblique to space-

Received June 20, 1992; revision received Aug. 24, 1993; accepted for publication Oct. 12, 1993.

*Senior Engineering Specialist, Space Systems Division. Senior Member AIAA.

craft principal axes, depending on the biases and frequency contents of the disturbances. Nonetheless, for all types of disturbances, an encompassing cylindrical momentum envelope can be determined for reaction wheel configuration optimization, considered in Sec. IV of the paper.

Regarding torque requirements for configuration optimization, these do not arise from the feeble environmental torques. Rather, they come from the aforementioned yaw steering or other slew requirements, attitude acquisition or reacquisition needs following the loss of Earth lock, reaction torques from articulated sensors (if any), etc., leading to a rectangular parallelepiped torque envelope (see DeBra and Cannon[4] and Cannon[5]). The associated momentum envelope must, of course, lie within the cylindrical momentum envelope already discussed. Having the torque and momentum envelopes thus specified, Fleming and Ramos[6] optimized the cant angle of a four-wheel pyramid configuration by requiring that when one wheel fails, the torque and momentum capacity of the remaining three wheels be the same, to generate equal roll and yaw and arbitrary pitch torque and a cylindrical momentum envelope about the pitch axis. Kral,[7] on the other hand, optimized the configuration geometry by minimizing the peak requirements on the wheels for a spherical momentum envelope, when only three noncoplanar wheels are active and the rest inactive. In this paper, in Sec. IV, the cant angle is optimized for minimum power consumption; four-, six-, and three-wheel configurations, with and without one wheel failure, are considered. Simple relationships are developed, relating momentum or torque requirements about the spacecraft axes to those about the wheel axes for all configurations, furnishing the required momentum and torque capacities of the wheels. The paper is finally concluded in Sec. V.

II. Commands for Sun Tracking

Coordinate Transformations

In this paper, we are concerned exclusively with circular orbits. The local-vertical-local-horizontal (LVLH) frame $\mathcal{F}^c$: X_c Y_c Z_c at any point in the orbit locates the spacecraft mass center, with X_c along the velocity vector, Z_c along the nadir, and Y_c opposite to the orbit normal. To maintain Earth pointing, the spacecraft rotates clockwise about the Y_c axis at the rate $-\omega_0$. The frame $\mathcal{F}^c$ is the standard roll, pitch, yaw frame of the spacecraft, with these three attitude angles being zero. When the angles are nonzero, the spacecraft frame is denoted $\mathcal{F}^0$: X_0 Y_0 Z_0 shown in Fig. 1. In this paper, however, we assume that the spacecraft is controlled perfectly, and it always maintains its ideal LVLH orientation.

We now define the orientation of two solar arrays relative to the frame $\mathcal{F}^c$ or, equivalently, $\mathcal{F}^0$. Each array turns relative to the spacecraft about a two-degree-of-freedom hinge (the hinges O_1 and O_2 in Fig. 1). Considering the $+Y$ array first (also called south array), its relative rotation is reckoned from the frame X_{10} Y_{10} Z_{10} parallel to the spacecraft frame $\mathcal{F}^0$. To track the sun, the first rotation of the array is θ_{1y} about the axis Y_{10}, cancelling the clockwise rotation $\omega_0 t$ of the Earth-pointing spacecraft measured from the ascending node line. The second rotation, earlier called β but denoted θ_{1z} from now on, takes place about the once displaced Z_{10} axis (or about the inboard transverse axis of the array). We then arrive at the array-fixed frame $\mathcal{F}^1$: X_1 Y_1 Z_1, with the array in the Y_1Z_1 plane and its outward normal along X_1. When the array is normal to the sun, the sun vector S from the sun to the Earth is opposite to the array normal X_1. Regarding the $-Y$ array (also called north array), its initial orientation is the same as that of the $+Y$ array, and the rotations of the $-Y$ array are conveniently measured from the frame $X_{20}Y_{20}Z_{20}$, with Y_{20} opposite to Y_0 and Z_{20} opposite to Z_0. The frames $X_{i0}Y_{i0}Z_{i0}$ ($i = 1, 2$) are positioned such that the solar cell faces of both arrays, normal to X_{i0} ($i = 1, 2$), are on the same side. The rotation θ_{2y} about the Y_{20} axis (Fig. 1) nullifies the orbit rotation, and the rotation θ_{2z} about the once displaced Z_{20} axis brings the array normal to the sun. The transformation matrices C_{0i} from the spacecraft frame $\mathcal{F}^0$ to the array-fixed frames $\mathcal{F}^i$: X_i Y_i Z_i ($i = 1, 2$) are furnished in Ref. 8.

Commands for Sun Tracking

Let S_{c1}, S_{c2}, and S_{c3} be the components of the sun-Earth vector S in $\mathcal{F}^c$. Using coordinate transformations involving the angles ν (the Earth's rotation around the sun in the ecliptic plane, measured from the first day of autumn, September 23), λ, Ω_N (the instantaneous ascending node of the orbit), i, and $\omega_0 t$, these components are found to be

$$S_{c1} = c\omega_0 t\{ci(-s\Omega_N c\nu + c\Omega_N c\lambda s\nu) + sis\lambda s\nu\} - s\omega_0 t(c\Omega_N c\nu + s\Omega_N c\lambda s\nu) \tag{1a}$$

$$S_{c2} = si(-s\Omega_N c\nu + c\Omega_N c\lambda s\nu) - cis\lambda s\nu \tag{1b}$$

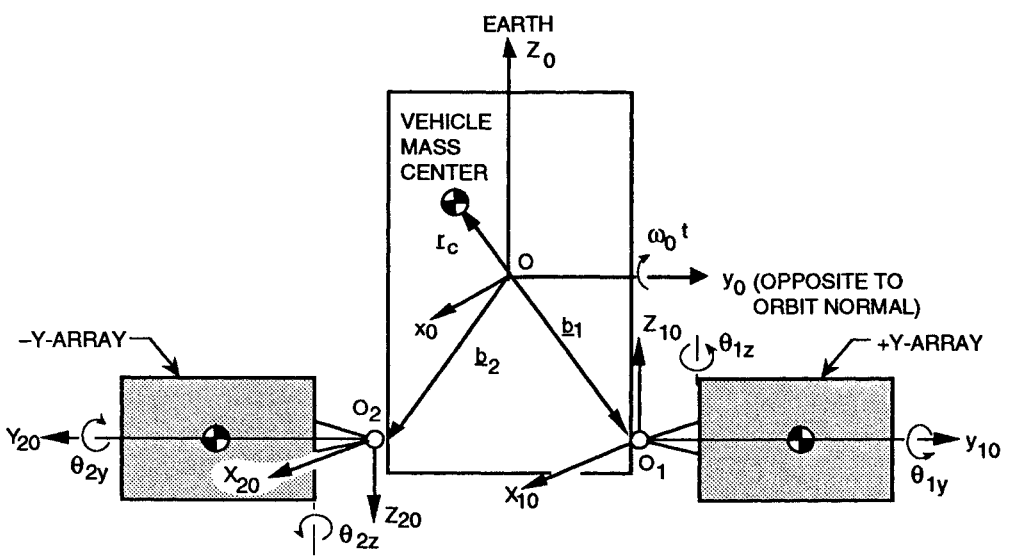

Fig. 1 Spacecraft with $+Y$ and $-Y$ arrays, their frames, and articulation degrees of freedom.

$$S_{c3} = -s\omega_0 t\{ci(-s\Omega_N cv + c\Omega_N c\lambda sv) + sis\lambda sv\} - c\omega_0 t(c\Omega_N cv + s\Omega_N c\lambda sv) \quad (1c)$$

where $c(\bullet) = \cos(\bullet)$ and $s(\bullet) = \sin(\bullet)$.

Y-Array Commands

Because the rotation θ_{1y} annuls the once-per-orbit rotation of the spacecraft, one must have

$$\theta_{1y}(t) = \omega_0 t + \theta_{10} \quad (2)$$

where θ_{10} is $\theta_{1y}(t = 0)$. Note that $\theta_{1y}(t)$ is anticlockwise positive, and the negative sign of the orbit rate is accounted for in Eq. (1), and so $\omega_0 t$ in Eq. (2) is positive. To determine θ_{10} and the second rotation θ_{1z}, recall that when the array is normal to the sun, the vector S is opposite to the outgoing array normal X_1. With the aid of the transformation matrix C_{01}, therefore,

$$[S_{c1} \quad S_{c2} \quad S_{c3}]^{\mathcal{F}0} = [-c\theta_{1y}c\theta_{1z} \quad -s\theta_{1z} \quad s\theta_{1y}c\theta_{1z}] \quad (3)$$

The initial angle θ_{10} is thereby determined by inserting Eq. (2) in Eq. (3) and recalling Eq. (1), yielding:

$$\theta_{10} = \tan^{-1}\frac{-[c\Omega_N cv + s\Omega_N c\lambda sv]}{-[ci(-s\Omega_N cv + c\Omega_N c\lambda sv) + sis\lambda sv]} \quad (4)$$

which is a unique value of θ_{10} within the range $-\pi \leq \theta_{10} \leq \pi$, and it ensures that the solar cell face of the array looks at the sun. The array's inclination angle θ_{1Z} is obtained from the second components of Eqs. (1) and (3)

$$\theta_{1z} = \sin^{-1}[si(s\Omega_N cv - c\Omega_N c\lambda sv) + cis\lambda sv] \quad (5)$$

Figure 2 illustrates the variation of θ_{10} and θ_{1Z} as a function of the Earth's position on the ecliptic plane ($0 \leq v \leq 2\pi$) for $i = 28.5$ deg and 11 values of the ascending node angle Ω_N. The apparent discontinuities in θ_{10} curves at $\pm\pi$ are not real, since $+\pi = -\pi$. The extrema of the angle θ_{1Z}, derived from Eq. (5), are summarized in Table 1. These extrema as well as the sinusoidal variation of the angle θ_{1z} with v are illustrated in Fig. 2.

If the ascending node angle Ω_N were constant, the angle θ_{1z} would vary sinusoidally over 1 yr, as shown in Fig. 2. And then, for a spacecraft with only one solar array having only θ_{1y} degree of freedom, the array would be fixed to the spacecraft at half the amplitude of the sinusoid, and once in every 6 months the spacecraft would be rotated by 180 deg about its yaw axis when θ_{1z} nears zero (that is, when the sun crosses the orbit plane). Because of the nodal regression, however, the angle Ω_N varies secularly; for example, for $i = 45$ deg, and altitude 926 km, the angle Ω_N changes westward by 5.2 deg/day in the equatorial plane, compared to the 0.986 deg/day eastward change of the angle v in the ecliptic plane. To combine the time dependence of Ω_N and v, Eq. (5) can be rewritten in terms of the right ascension α, in the equatorial plane, of the sun and declination δ, defined as

$$s\delta = s\lambda sv, \qquad c\delta s\alpha = c\lambda sv, \qquad c\delta c\alpha = cv \quad (6)$$

which transforms Eq. (5) to

$$\theta_{1z} = \sin^{-1}[sic\delta s(\Omega_N - \alpha) + cis\delta] \quad (7)$$

Although the angle δ varies between $-\lambda$ and λ in 1 yr and the angle α varies between 0 and 2π, the angle $(\Omega_N - \alpha)$ varies from 0 to 2π several times in a year, due to nodal regression. Thus the angle θ_{1z} varies within the range $-(\lambda + i) \leq \theta_{1z} \leq$

Table 1 Extrema of the tilt angle θ_{1z}

Earth's position on the ecliptic plane (v, deg; $v = 0$ = autumn equinox)		Ascending node angle of the spacecraft orbit (Ω_N, deg)	Extremum of θ_{1z}
90	winter solstice	0	$\lambda - i$
90	winter solstice	180	$\lambda + i$
−90 (or 270)	summer solstice	0	$i - \lambda$
−90 (or 270)	summer solstice	180	$-\lambda - i$

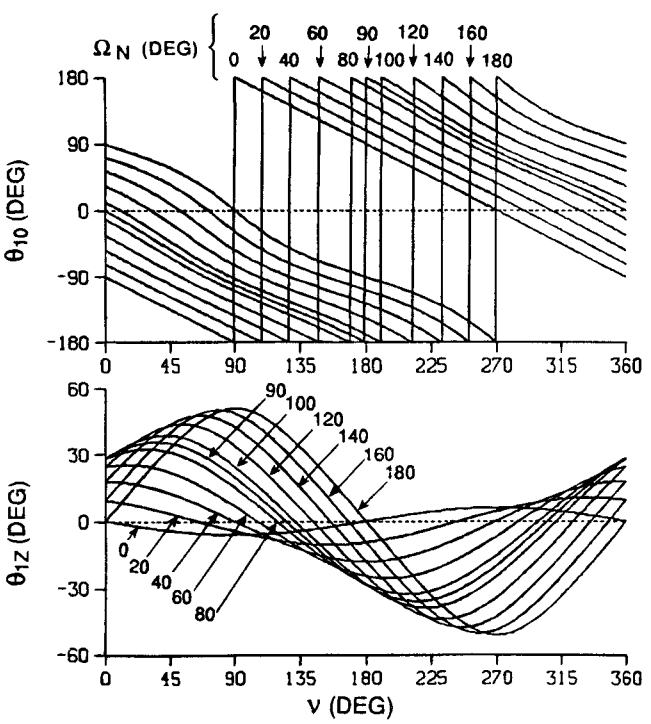

Fig. 2 Initial angle θ_{10} about the pitch axis Y_0 and the inclination angle θ_{1z} about the Z_1 axis of $+Y$ array. $i = 28.5$ deg, $\lambda = 23.44$ deg.

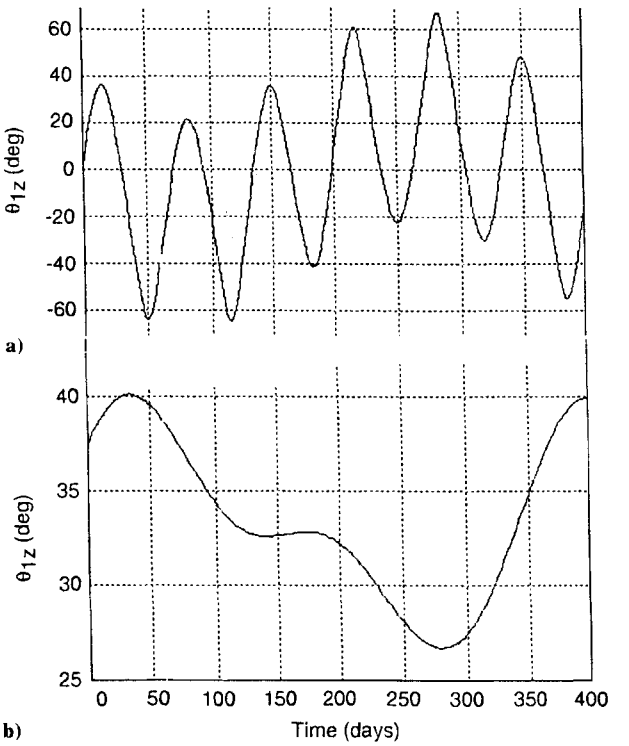

Fig. 3 Angle θ_{1z} vs days: a) $h = 926$ km, $i = 45$ deg, $v(t = 0) = 5.4$ deg, $\Omega_N(t = 0) = 0$ deg, and b) sun-synchronous orbit, $h = 833.4$ km, $i = 98.74$ deg, $v(t = 0) = 5.4$ deg, $\Omega_N(t = 0) = 223$ deg.

$(\lambda + i)$ with two frequencies: nodal regression frequency and the frequency corresponding to 1-yr period (see Fig. 3a). Furthermore, for the parameters in Fig. 3a, a spacecraft with one solar array, fixed at θ_{1z} near $(\lambda + i)/2$, will require a 180-deg yaw rotation nearly every month. In contrast, for sun-synchronous orbits, the orbit inclination i (necessarily greater than 90 deg) and the spacecraft altitude are both selected such that the eastward rate (because $i > 90$ deg) $\dot{\Omega}_N$ of the nodal movement cancels the rate $\dot{\alpha}$ of the sun's apparent motion in the equatorial plane; consequently, the angle $(\Omega_N - \alpha)$ remains essentially constant, equal to its initial value, throughout the year. Correspondingly, the angle θ_{1z} varies within a narrow range about some nominal value, because of the variation in the sun's declination angle δ over a year. Figure 3b illustrates this variation. Clearly, then, for a spacecraft in a sun-synchronous orbit, it is adequate to have just one array at a mean, fixed θ_{1z}, without requiring a yaw rotation and without enduring a significant power loss due to the off normality of the sun rays over one year.

−Y-Array Commands

In accordance with the definitions of the angles θ_{2y} and θ_{2z} already stated, it is clear that for keeping the $-Y$-array normal to the sun rays

$$\theta_{2y} = -\theta_{1y} \tag{8a}$$

$$\theta_{2z} = -\theta_{1z} \tag{8b}$$

Recalling Eq. (2), the desired $\theta_{2y}(t)$ will therefore be $\theta_{2y}(t) = -\omega_0 t - \theta_{10}$.

III. Solar Radiation Torque and Momentum Accumulation

Solar Radiation Torque

Complex geometry of most real spacecraft is not amenable to a literal analysis of solar radiation torque and momentum accumulation. Spacecraft buses with polygonal, varying cross-sectional geometries, protruding antennas and scientific instruments, shadowing of the bus by the solar arrays and vice versa, sun eclipses for low-altitude orbits, and so forth, necessitate computer analyses for an accurate assessment of the torque and momentum accumulation. Nevertheless, the fact remains that certain basic features of these results can be arrived at—indeed must be known a priori for an independent validation of the computer results—by considering the torque caused by the arrays only. Furthermore, simple expressions of momentum accumulation over an orbit prove handy in sizing the wheels. Evans[9] and Ref. 8 consider the shadowing of the arrays by the bus, the attendant variation in the arrays' lit area, the center of pressure movement, and the corresponding variation in the moment arm from the instantaneous center of mass to the instantaneous center of pressure. However, at least for the spacecraft program that led to this study, it is found that, although the radiation torque changes significantly during the mutual shielding period, the overall change in the momentum accumulation (the quantity that really matters) is insignificant, because the shadow area builds slowly to its maximum value and then recedes. Therefore, next we record the solar radiation torque $\boldsymbol{g}^{\mathcal{F}^c}$ in the frame $\mathcal{F}^c$, acting at the spacecraft's mass center, due to the $+Y$ array normal to the sun and $-Y$ array off normal, ignoring mutual shadowing and torque on the bus:

$$\boldsymbol{g}^{\mathcal{F}^c} = [g_c + g_a s\theta_{1y} \quad g_b c\theta_{1y} \quad g_a c\theta_{1y}]^T \tag{9}$$

Here, g_a, g_b, and g_c are constant over some orbits and the roll and yaw torques vary in quadrature. Equation (9) is based on the additional assumption that the hinges O_1 and O_2 (Fig. 1) are in the pitch-yaw plane; that is, the hinge vectors $-\boldsymbol{r}_c + \boldsymbol{b}_i$ $(i = 1, 2)$ have no roll components. The detailed derivation of Eq. (9) and the definitions of the quasi-constants g_a, g_b, and g_c are given in Ref. 8. Because of the sun-tracking command Eq. (2), the roll/yaw torque components in Eq. (9) vary at orbit frequency. But the solar torque is not necessarily limited to this frequency, for if an articulated, Earth-pointing antenna were considered, the attendant solar torque would vary at twice the orbit frequency. Similarly, other disturbance torques give rise to different multiples of orbit frequency. Thus, the torque expression (9) is valid only for sun-pointing solar arrays attached to an Earth-pointing spacecraft, with the vector from the vehicle's mass center to the array's pressure center in the pitch-yaw plane.

Momentum Accumulation

Let $\boldsymbol{H}_b$ be the excess angular momentum vector of the Earth-pointing spacecraft. If H_x, H_y, and H_z denote the components of $\boldsymbol{H}_b$ in the body-fixed frame $\mathcal{F}^0$, then, under the radiation torque (9), one can readily show that

$$H_x + jH_z = -j(g_c/\omega_0)(1 - e^{-j\omega_0 t}) + jtg_a e^{-j\omega_0 t} \tag{10}$$

$$H_y(t) = (g_b/\omega_0)\sin\omega_0 t \tag{11}$$

where $j^2 = -1$, and the time t is reckoned from the instant $\theta_{1y} = 0$ (not ascending node). The secular momentum tg_a in the roll/yaw (orbit) plane, due to the torque g_a constant in the inertial frame, is the instantaneous radius of the circular spiral. Depending on the initial conditions, this secular momentum, when momentum removal commences, can be either about the roll axis, yaw axis, or any other direction in the roll-yaw plane. Therefore, if τ_{md} is the duration between two consecutive momentum removal operations, the desired momentum capacity in the roll-yaw plane is a circle of radius $\tau_{md} g_a \triangleq H_{x/z}$. Maximum amplitude of the cyclic term in Eq. (10) is $2g_c/\omega_0$ at $\omega_0 t = \pi$, but it is assumed that in the duration $0 < t < \tau_{md}$, $|H_x + jH_z| < H_{x/z}$. The amplitude of the cyclic pitch momentum is equal to $H_y \triangleq g_b/\omega_0$.

As stated in the Introduction, for atmospheric, magnetic, or gravity gradient torques, the frequency contents and the bias components are different from those in Eq. (9), and the corresponding roll/yaw momentum spiral is usually skewed and elliptic. But for the reaction wheel configuration optimization, we assume that the required momentum envelope is cylindrical, with the semilength H_y and radius $H_{x/z}$, determined as illustrated earlier. The aspect ratio $H_y/H_{x/z}$ for the spacecraft shown in Fig. 1, with Y array normal to the sun and $-Y$ array off normal by an angle $\delta_{2z} \triangleq \theta_{2z} - \theta'_{2z}$, is illustrated in Fig. 4 for a 24-h orbit with constant Ω_N and i. Here, the angle θ'_{2z} is the actual angle of the $-Y$ array and θ_{2z} is the angle for the array to be normal to the sun. Moreover, the assumption of constant Ω_N is justified because for a 24-h orbit with $i = 28.5$ deg, the westward nodal regression is merely 0.0118 deg/day (4.3 deg/yr). We observe in Fig. 4 that, when both arrays are normal ($\delta_{2z} = 0$), the aspect ratio $H_y/H_{x/z}$ is constant for all seasons of the year. However, as the off normality (the angle δ_{2z}) increases, the ratio $H_y/H_{x/z}$

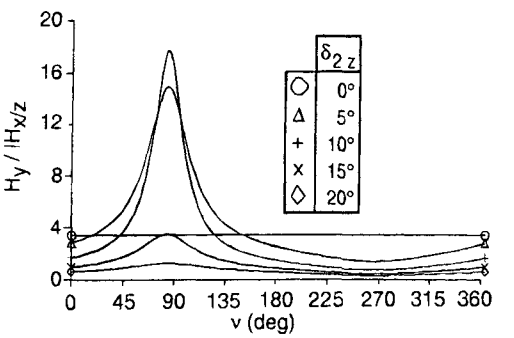

Fig. 4 Ratio between pitch momentum and roll/yaw momentum vs the angle ν. $i = 28.5$ deg, $\Omega_N = 170$ deg, $\lambda = 23.44$ deg, orbit period = 24 h.

begins to vary considerably with the angle ν, thereby suggesting that the size of the cylindrical momentum envelope varies throughout the year. For further details on this example and the analysis concerning yearly momentum accumulation, see Ref. 8.

IV. Reaction Wheel Sizing and Configuration Optimization

We just observed that the momentum envelope arising from external disturbances, acting on an Earth-pointing spacecraft, is cylindrical, or can be approximated so, with its longitudinal axis along the pitch axis and circular cross section in the orbit plane. On the other hand, as stated in the Introduction, the torque envelope to be delivered by the wheels is usually a rectangular parallelepiped. The associated momentum envelope is also a rectangular parallelepiped, but entirely within the cylindrical envelope associated with the external disturbances. Both the momentum and the torque requirements can be met using three wheels (not necessarily orthogonal), but for the sake of redundancy, four or more are often employed. To visualize the wheel configuration most easily, first place the spin axes of all of the wheels in the roll-yaw plane, radially symmetrically along the roll and yaw axes or otherwise, and then cant all spin axes, equally or unequally depending on the design, toward the pitch axis or its opposite. This orientation is not ideal for all circumstances; for example, for the TOPEX spacecraft[2] the four-wheel pyramid axis is along the yaw (z) axis to facilitate the yaw rotations of the spacecraft for sun tracking. On the other hand, for the inertially-stabilized Gamma Ray Observatory, the pyramid axis is along the spacecraft x axis.[10] The formulas developed subsequently, however, can be used for any such arrangement by reinterpreting the x, y, z subscripts appropriately.

When the wheels are not along the spacecraft axes, a transformation matrix $\boldsymbol{C}_{bw}$ transforms the wheel momentum vector $\boldsymbol{H}_{ww}$ along the wheel axes to the total wheel momentum $\boldsymbol{H}_{bw}$ along the spacecraft axes

$$\boldsymbol{H}_{bw} = \boldsymbol{C}_{bw}\boldsymbol{H}_{ww} \tag{12}$$

When the number of wheels n_w is more than 3, the matrix $\boldsymbol{C}_{bw}$ is rectangular, $3 \times n_w$, and its pseudoinverse

$$\boldsymbol{C}_{bw}^{\dagger} = \boldsymbol{C}_{bw}^{T}(\boldsymbol{C}_{bw}\boldsymbol{C}_{bw}^{T})^{-1} \tag{13}$$

is required for the inverse transformation of Eq. (12)

$$\boldsymbol{H}_{ww} = \boldsymbol{C}_{bw}^{\dagger}\boldsymbol{H}_{bw} \tag{14}$$

The preceding two transformation matrices are also useful for transforming the desired, known control torque $\boldsymbol{T}_c$ (3×1) about the spacecraft axes to the desired rate of change of the wheel angular momentum vector $\dot{\boldsymbol{H}}_{ww}$ ($n_w \times 1$)

$$\dot{\boldsymbol{H}}_{ww} = -\boldsymbol{C}_{bw}^{\dagger}\boldsymbol{T}_c \tag{15}$$

To optimize the cant angle(s) of the wheels with the roll-yaw plane, it appears logical to require that, for a desired momentum vector capacity $\boldsymbol{H}_{bw}$ in spacecraft axes, the norm of the wheel momentum vector $\boldsymbol{H}_{ww}$ be the least so as to minimize the cost and weight of the wheels and, as shown later, power consumption. Notwithstanding this approach, however, Fleming and Ramos[6] invoke a different optimization criterion, elaborated in the last subsection wherein we also compare the optimum angle derived here with that in Ref. 6. In any event, a suitable norm of the vector $\boldsymbol{H}_{ww}$ is its Euclidean norm $\|\boldsymbol{H}_{ww}\|$ defined by

$$\|\boldsymbol{H}_{ww}\| = \left[\sum_{i=1}^{n_w} H_{wi}^2\right]^{1/2} \tag{16}$$

where H_{wi} ($i = 1, \ldots, n_w$) is the angular momentum of the wheel i. The minimization of $\|\boldsymbol{H}_{ww}\|$ also results in minimum power consumption by the wheels, for letting $\omega_w(0)$ be the nominal speed of the wheels (the same for each wheel), I_w the moment of inertia of each wheel about its spin axis, and $\dot{H}_{wi}$ be the constant torque produced by the ith wheel, Ref. 8 then shows that the power P_w consumed by the wheel assembly is

$$P_w = |\omega_w(0)| \sum_{i=1}^{n_w} |\dot{H}_{wi}| + tI_w^{-1}\|\dot{\boldsymbol{H}}_{ww}\|^2 \tag{17}$$

For reaction wheels, a low, nominal speed $\omega_w(0)$ is maintained to avoid the sticking of the wheels to the bearings due to friction; power is thus lost in counteracting the frictional torques. Additional power is consumed by the wheel electronics. The sum total of these losses is significant, but it is not considered here. Furthermore, for momentum bias satellites, the nominal speed $\omega_w(0)$ is typically a few thousand rpms, and so both terms in the right-hand side (rhs) of Eq. (17) become significant. However, in the case of nominally zero-momentum satellites of concern here, $\omega_w(0)$ is likely to be small, if not zero, and therefore the first rhs term in Eq. (17) is negligible compared to the second term. Admittedly, this is not always true, as individual wheels can have positive and negative high speeds such that the net momentum of the assembly is zero, and yet the first rhs term in Eq. (17) is significant. In any event, with mathematical convenience in view, the secular growth of the second term in the rhs of Eq. (17) lures us to conclude that the minimization of the power consumption P_w amounts to the minimization of the norm $\|\dot{\boldsymbol{H}}_{ww}\|$. Finally, the minimization of both $\boldsymbol{H}_{ww}$ and $\dot{\boldsymbol{H}}_{ww}$ will yield the same optimum cant angle only if the components of $\boldsymbol{H}_{bw}$ and $\boldsymbol{T}_c$ are proportional; but this may not always be the case. We saw one example of this in Fig. 4 where the aspect ratio of the cylindrical momentum envelope is found to change over a year. In such circumstances, a compromise must be sought. Several wheel configurations are now considered for optimization.

Four-Wheel Pyramid Configurations: $\gamma = 0$ or 45 deg

One possible arrangement of four reaction wheels is shown in Fig. 5. The angle between any two adjacent wheels is 90 deg, and they are all canted equally toward the $-y$ axis by an angle η measured from the roll-yaw plane. When the cant angle η and the angle γ in the roll-yaw-plane are both zero, the momentum h_1 of the wheel 1 is along the z axis, h_2 along the x axis, h_3 opposite to h_1, and h_4 opposite to h_2. For $\gamma = 45$ deg,

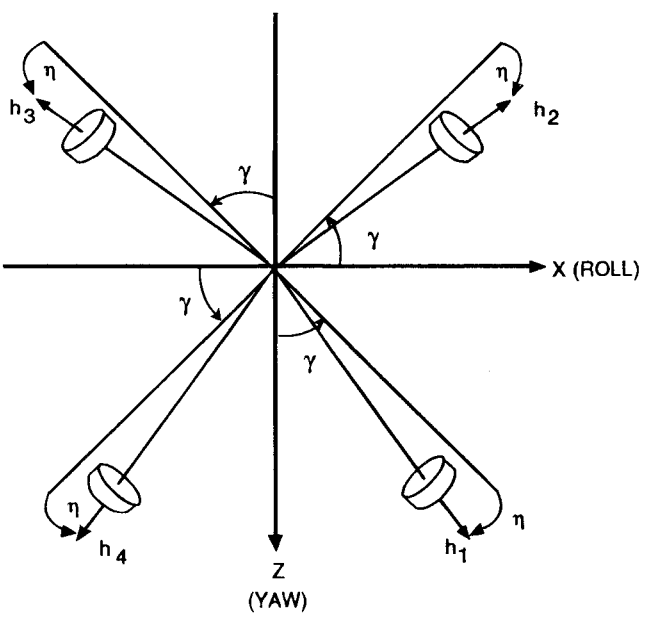

Fig. 5 Four-wheel configuration ($\gamma = 0$ or 45 deg).

this configuration becomes the one considered by Fleming and Ramos,[6] and each wheel then controls all three axes. On the other hand, for $\gamma = 0$, each wheel controls either roll and pitch or yaw and pitch.

Let (H_x, H_y, H_z) and (T_x, T_y, T_z), respectively, be the desired momentum and torque capacity of the reaction wheels about the spacecraft X_o, Y_o, and Z_o axes. Using Eqs. (12–16), one can show that the norms $\|\boldsymbol{H}_{ww}\|$ and $\|\dot{\boldsymbol{H}}_{ww}\|$ are

$$\|\boldsymbol{H}_{ww}\|^2 = (H_x^2 + H_z^2)/(2c^2\eta) + H_y^2/(4s^2\eta) \tag{18}$$

$$\|\dot{\boldsymbol{H}}_{ww}\|^2 = (T_x^2 + T_z^2)/(2c^2\eta) + T_y^2/(4s^2\eta) \tag{19}$$

These are independent of the angle γ because the angle between any two adjacent wheels is 90 deg. Also, as expected, both norms become infinite when η approaches zero (no wheels for pitch control) or 90 deg (no wheels for roll and yaw control). Obviously, these singular configurations are useless for three-axis control. Returning to the normal case, the optimum cant angle η^* for the minimum norm, derived from Eqs. (18) and (19), is

$$\tan^4 \eta^* = H_y^2/2(H_x^2 + H_z^2) = T_y^2/2(T_x^2 + T_z^2) \tag{20}$$

Equation (20) states that as the torque requirements about the x_0 and z_0 axis diminish, the optimum cant angle η^* increases. It furthermore reveals that although this configuration is aptly suited for a cylindrical momentum envelope $H_x^2 + H_z^2 = H_{x/z}^2$ is precisely the equation of a circle), it is unsuitable for unequal torque ratios T_x/T_y and T_z/T_y, because the optimum angle η^* depends on the sum of the squares of these two ratios, not on the individual ratios. In a more versatile configuration considered subsequently and shown in Fig. 6, each wheel will have an angle γ with the roll axis and $(90 - \gamma)$ deg with the yaw axis. Continuing with the wheel configuration of Fig. 5, the minimum value of the norm occurs at η^* and, using Eq. (20), it is found to be

$$\|\dot{\boldsymbol{H}}_{ww}\|^2_{\min}/T_y^2 = [\sqrt{2}(\sigma_{xy}^2 + \sigma_{zy}^2)^{1/2} + 1]^2/4 \tag{21}$$

where $\sigma_{xy} \triangleq T_x/T_y$ and $\sigma_{zy} = T_z/T_y$.

To determine the torque (or momentum) capacity of the wheels for producing the desired torque components (or momenta) along the spacecraft axes, the Euclidean norm is not helpful, and so we now focus on the vector $\dot{\boldsymbol{H}}_{ww}$ itself.

Each Wheel Controlling Either Roll and Pitch or Yaw and Pitch ($\gamma = 0$ deg)

According to Eq. (20), the optimum cant angle, regardless of γ, for equal torque and momentum requirements is

$$\eta^* = 35.26 \text{ deg}, \qquad \tan \eta^* = 1/\sqrt{2} \tag{22a}$$

$$\sin \eta^* = 1/\sqrt{3}, \qquad \cos \eta^* = \sqrt{2/3} \tag{22b}$$

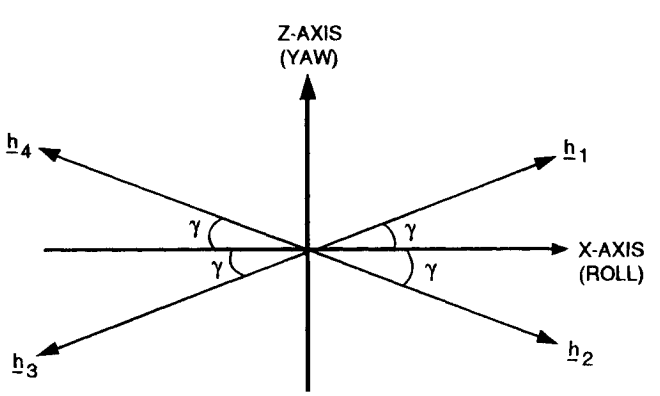

Fig. 6 Four-wheel configuration for unequal torque requirements: roll/yaw plane.

Substituting $T_x = T_y = T_z$, $\gamma = 0$ deg, and $s\eta^*$ and $c\eta^*$ from Eq. (22b) in Eq. (15), we obtain

$$\dot{\boldsymbol{H}}_{ww} = T_x[-0.179 \quad 1.045 \quad 1.045 \quad -0.179]^T \tag{23}$$

from which the second and the third element yield the required wheel torque capacity, without wheel-failure

$$\dot{H}_{w,\,mx} \geq 1.045\, T_x \tag{24}$$

To determine the required momentum capacity of the wheels, we recall that for a cylindrical momentum envelope with radius $H_{x/z}$ and semilength H_y, the secular momentum about either the roll or yaw axis, not concurrently, is $H_{x/z}$ and the pitch momentum amplitude is H_y. Using Eq. (14) for $\gamma = 0$ deg and $\eta = \eta^*$, the following momentum capacity of a wheel is then arrived at

$$H_{w,\,mx} \geq \sqrt{3}\, H_{x/z}/2\sqrt{2} + \sqrt{3}\, H_y/4 \tag{25}$$

Finally, to calculate the power consumption P_w for equal torque requirement about the three axes, the quantities $\sum_{i=1}^{n_w} |\dot{H}_{wi}|$ and $\|\dot{\boldsymbol{H}}_{ww}\|^2$, using Eqs. (23) and (21), are found to be

$$\sum_{i=1}^{n_w} |\dot{H}_{wi}| = 2.449\, T_x \tag{26a}$$

$$\|\dot{\boldsymbol{H}}_{ww}\|^2 = 2.25\, T_x^2 \tag{26b}$$

Each Wheel Controlling All Three Axes ($\gamma = 45$ deg)

For equal torque requirement ($T_x = T_y = T_z$) and optimum cant angle [Eq. (22)], Eq. (15) yields $\dot{\boldsymbol{H}}_{ww}$, from which the element with the maximum absolute value furnishes the required torque capacity of the wheels

$$\dot{H}_{w,\,mx} \geq 3\sqrt{3}\, T_{mx}/4 = 1.3\, T_x \tag{27}$$

Comparing Eq. (27) with Eq. (24), we conclude that, to produce a torque of magnitude T_x about each of the three axes, the reaction wheels of a 45-deg configuration must have 24.4% higher torque capacity than the wheels of a 0-deg configuration, because for $\gamma = 45$ deg the wheel's torque is dispersed along all three axes, whereas for $\gamma = 0$ deg, it is dispersed along the roll and pitch or yaw and pitch only.

Regarding the momentum capacity, the vector $\boldsymbol{H}_{ww}$ is found to have the terms $(H_x + H_z)$ whose largest magnitude for a cylindrical momentum envelope with $H_{x/z}$ radius in the roll/yaw plane is $\sqrt{2}\, H_{x/z}$. (This was not realized in Ref. 8, and, consequently, there is a difference of $\sqrt{2}$ between the first terms of the right-hand sides of Eq. (29) here and Eq. (86), Ref. 8.) Therefore, the wheel momentum capacity furnished by the largest element of $\boldsymbol{H}_{ww}$ is

$$H_{w,\,mx} = H_{x/z}/(2c\eta) + H_y/(4s\eta) \tag{28}$$

When the optimum cant angle, Eqs. (22), for equal torque requirement is used, Eq. (28) yields

$$H_{w,\,mx} = \sqrt{3}\, H_{x/z}/2\sqrt{2} + \sqrt{3}\, H_y/4 \tag{29}$$

which, not surprisingly, is the same as Eq. (25), because the four-wheel configuration at hand is expressly for a cylindrical momentum envelope regardless of the angle γ.

Regarding the two indexes of power consumption for equal torque requirement, one arrives at

$$\sum_{i=1}^{4} |\dot{H}_{wi}| = 2.598\, T_x \tag{30a}$$

$$\|\dot{\boldsymbol{H}}_{ww}\|^2 = 2.25\, T_x^2 \tag{30b}$$

Comparing Eq. (30) with Eq. (26), we infer that, for producing equal torque about the three spacecraft axes and for the same initial wheel speed, the 45-deg configuration starts with a slightly higher power consumption than the 0-deg configuration does, but both power consumptions increase at the same rate.

One-Wheel Failure

For the four-wheel configuration shown in Fig. 5, with γ = 0 or 45 deg, because all wheels are arranged symmetrically, the failure of any wheel has the same consequence as the failure of any other. Therefore, we arbitrarily assume the failure of wheel 3, and degenerate the 3 × 4 transformation matrix $\boldsymbol{C}_{bw}$ to a 3 × 3 matrix $\boldsymbol{C}_{bw,3}$ formed by deleting the third column of $\boldsymbol{C}_{bw}$. The inverse $\boldsymbol{C}_{bw,3}^{-1}$ is then used to determine the torque vector $\dot{\boldsymbol{H}}_{ww}$ and the wheel momentum vector $\boldsymbol{H}_{ww}$. For the wheel failure case, the cant angle is not reoptimized because once the wheels are installed, their cant angle is not changed in the orbit. The optimization approach of Fleming and Ramos[6] is different, though, in that they optimize the cant angle specifically for a one-wheel-failure situation.

Maximum Torque and Momentum Capacity When γ = 0 deg

For γ = 0 deg and the optimum cant angle Eqs. (22), $\dot{\boldsymbol{H}}_{ww}$ yields the required torque capacity of the wheel as

$$\dot{H}_{w,\,mx} \geq 2.091\ T_x \tag{31}$$

which is twice the capacity [Eq. (24)] for the no-failure case. To determine the momentum capacity, we again evaluate $\boldsymbol{H}_{ww}$ using Eq. (14) where we replace $\boldsymbol{C}_{bw}^{\dagger}$ with $\boldsymbol{C}_{bw,3}^{-1}$, and arrive at

$$\boldsymbol{H}_{ww} = [H_{x/z}/c\eta \quad H_{x/z}/(\sqrt{2}\,c\eta) + H_y/(2s\eta) \quad 0 \quad H_{x/z}/(\sqrt{2}\,c\eta) + H_y/(2s\eta)]^T \tag{32}$$

The wheel momentum capacity, therefore, must be

$$H_{w,\,mx} = \max[H_{x/z}/c\eta,\quad H_{x/z}/(\sqrt{2}\,c\eta) + H_y/(2s\eta)] \tag{33}$$

which may be compared with Eq. (28).

Regarding the two indices of power consumption, the vector $\dot{\boldsymbol{H}}_{ww}$ furnishes

$$\sum_{i=1}^{4} |\dot{H}_{wi}| = 4.182\ T_x, \qquad \|\dot{\boldsymbol{H}}_{ww}\|^2 = 6.62\ T_x^2 \tag{34}$$

It is worthwhile comparing Eqs. (34) with Eqs. (30).

Maximum Torque and Momentum Capacity When γ = 45 deg

For equal torque components about the roll, pitch, and yaw axes and the optimum cant angle η^* = 35.26, the required torque capacity of each wheel is found to be

$$\dot{\boldsymbol{H}}_{w,\,mx} \geq 1.732\ T_x \tag{35}$$

which agrees with the result in Fig. 5 of Ref. 6 (also see the next subsection). Furthermore, compare Eq. (35) with the no-failure size Eq. (27). Comparing the torque capacities Eqs. (31) and (35), the advantage of the 45-deg configuration over the 0-deg configuration emerges: when one wheel fails, the 45-deg configuration can control the spacecraft with the wheels of smaller torque capacity than the 0-deg configuration can. The two indices of power consumption are

$$\sum_{i=1}^{4} |\dot{H}_{wi}| = 3\sqrt{3}\ T_x = 5.196\ T_x, \qquad \|\dot{\boldsymbol{H}}_{ww}\|^2 = 9\ T_x^2 \tag{36}$$

A comparison of Eq. (36) with Eq. (34) brings out a disadvantage of the 45-deg configuration: with one wheel failed, its power consumption is significantly greater than that of the 0-deg configuration. The required momentum capacity, however, is found to be the same as that for the 0-deg configuration, Eq. (33).

Optimization for One-Wheel Failure: γ = 45 deg

As stated earlier, the cant angle in Ref. 6 is not optimized for minimum power consumption; instead, it is expressly optimized for a one-wheel-failure scenario. Assuming that the roll and yaw torque requirements are equal ($T_x = T_z$) and defining (following Ref. 6) $a_T \triangleq T_y/T_x = 1/\sigma_{xy} = 1/\sigma_{zy}$, the magnitude of each element of the wheel torque vector $\dot{\boldsymbol{H}}_{ww}$ is found to be, using Eq. (15) and replacing $C_{bw}^{\dagger}$ with $C_{bw,3}^{-1}$,

$$\dot{\boldsymbol{H}}_{ww} = T_x[\sqrt{2}/c\eta \quad a_T/(2s\eta) + 1/(\sqrt{2}\,c\eta) \quad 0 \quad a_T/(2s\eta) + 1/(\sqrt{2}\,c\eta)]^T \tag{37}$$

For a specified torque ratio a_T, Fleming and Ramos[6] call that cant angle η_T torque optimal for which the torque capacity of each wheel in Eq. (37) is the same, leading to

$$\tan \eta_T = a_T/\sqrt{2} \tag{38}$$

In contrast, due to the assumption $T_x = T_z$, the optimum angle η^*, Eq. (20), simplifies to

$$\tan \eta_T^* = \sqrt{a_T}/\sqrt{2} \tag{39}$$

Thus, the angles η_T and η_T^* are different unless $T_x = T_y = T_z$, that is, $a_T = 1$.

On the other hand, to optimize for momentum, consider the vector $\boldsymbol{H}_{ww}$ given by Eq. (32), valid for both γ = 0 and 45 deg. For a cylindrical momentum envelope of radius $H_{x/z}$ and semilength H_y, Fleming and Ramos[6] define the aspect ratio a_H as $a_H = H_y/H_{x/z}$ and call that cant angle η_H momentum optimum for which the two choices of the momentum capacity in Eq. (32) are equal, furnishing

$$\tan \eta_H = a_H/(2 - \sqrt{2}) \tag{40}$$

But, for the same cylindrical momentum envelope, the minimum power consumption optimum angle η^*, Eq. (20), produces

$$\tan \eta_H^* = \sqrt{a_H}/2^{1/4} \tag{41}$$

Thus, generally, the four optimum angles η_T, η_T^*, η_H, and η_H^* are all different. See Fig. 5, Ref. 6, for an illustration of the approach.

Four-Wheel Configuration for Unequal Roll/Yaw Torque Requirements

Figure 6 depicts a four-wheel configuration, more suitable than the one in Fig. 5 for unequal roll and yaw torque requirements because the angle γ is now general and can be selected to suit the roll/yaw torque requirements at hand. (Note that γ = 0 deg in Fig. 5 is not the same as γ = 0 deg in Fig. 6.) Following the given optimization procedure, it can be shown that the optimum angles γ^* and η^* for minimum power consumption are

$$\tan^2 \gamma^* = T_z/T_x \tag{42a}$$

$$\tan^2 \eta^* = T_y/(T_x + T_z) \tag{42b}$$

which, for $T_x = T_z$, yield γ^* = 45 deg and η^* equal to that given by Eq. (20), arriving at the 45 deg configuration considered earlier. Furthermore, the torque and momentum capacity of each reaction wheel, the latter for cylindrical momentum envelope, are found to be

$$\dot{H}_{w,\,mx} = \tfrac{1}{4}\,(\sqrt{T_x} + \sqrt{T_y} + \sqrt{T_z})\,\sqrt{T_x + T_y + T_z} \tag{43}$$

$$H_{w,\,mx} = \tfrac{1}{4}\,(2^{3/4}\sqrt{H_{x/z}} + \sqrt{H_y})\sqrt{H_y + \sqrt{2}\,H_{x/z}} \tag{44}$$

For equal torque requirement, Eq. (43) reduces to the torque capacity Eq. (27). Under one-wheel-failure scenario, the wheel torque and momentum capacities must be raised to

$$\dot{H}_{w,\,mx} = \tfrac{1}{2}\max[(\sqrt{T_x} + \sqrt{T_y}),\,(\sqrt{T_y} + \sqrt{T_z}),\,(\sqrt{T_z} + \sqrt{T_x})]\,\sqrt{T_x + T_y + T_z} \tag{45}$$

$$H_{w,\,mx} = \tfrac{1}{2}\max[(\sqrt{H_{x/z}} + \sqrt{H_y}),\quad 2^{3/4}\sqrt{H_{x/z}}]\sqrt{H_y + \sqrt{2}\,H_{x/z}} \tag{46}$$

Again, for equal torque components, Eq. (45) yields the torque capacity Eq. (35) for the 45-deg configuration.

Six-Wheel Pyramid Configuration

One such configuration is shown in Fig. 7 where the wheels are arranged symmetrically ($\gamma = 60$ deg), wheels 2 and 5 controlling the roll and pitch axes, and wheels 1, 3, 4, and 6 controlling all three axes. Because of this fundamental difference between the two subsets of wheels, the cant angle η_2 of the former subset is allowed to be different from the cant angle η_1 of the latter subset. This freedom permits (1) the unequal roll/pitch/yaw torque requirement, (2) greater economy in the power consumption, and (3) reaction wheels of smaller torque and momentum capacity than the one-cant-angle configuration allows.

To determine the optimum cant angles η_1^* and η_2^* define $c_i = \cos\eta_i$, and $s_i = \sin\eta_i$ (i = 1,2). Reference 8 then shows that the Euclidean norm of the vector $\dot{\boldsymbol{H}}_{ww}$ is

$$\|\dot{\boldsymbol{H}}_{ww}\|^2 = T_x^2/(c_1^2 + 2c_2^2) + T_y^2/2(2s_1^2 + s_2^2) + T_z^2/3c_1^2 \tag{47}$$

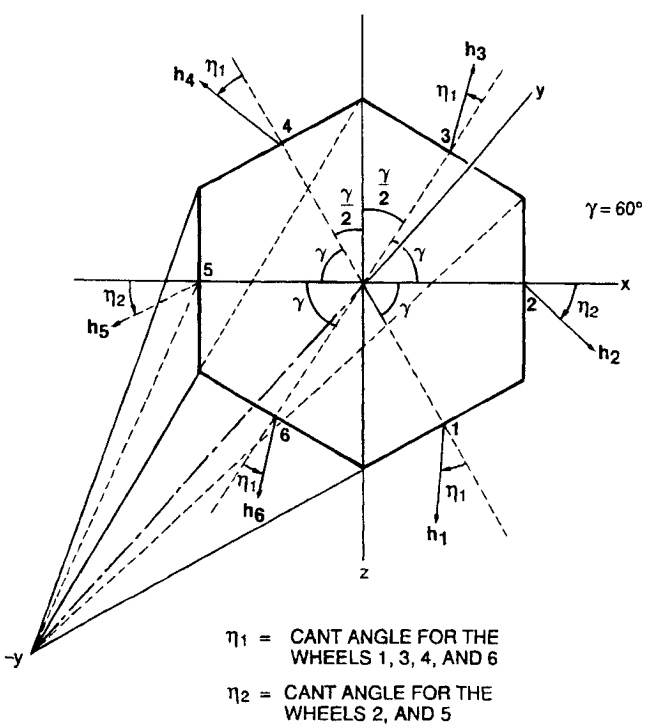

η_1 = CANT ANGLE FOR THE WHEELS 1, 3, 4, AND 6

η_2 = CANT ANGLE FOR THE WHEELS 2, AND 5

Fig. 7 Six-wheel hexagonal configuration.

which is minimized by the optimum angles η_1^* and η_2^* defined by

$$s^2\eta_1^* = (T_x + T_y - T_z)/(T_x + T_y + T_z)$$
$$c^2\eta_1^* = 2T_z/(T_x + T_y + T_z) \tag{48}$$

$$s^2\eta_2^* = \{2(T_z - T_x) + T_y\}/(T_x + T_y + T_z)$$
$$c^2\eta_2^* = (3T_x - T_z)/(T_x + T_y + T_z) \tag{49}$$

where $T_x \geq 0$, $T_y \geq 0$, and $T_z \geq 0$. For the equal torque requirement, the two cant angles coalesce and become the same as that for the four-wheel configurations. The required torque capacity of the wheels, then, is

$$\dot{H}_{w,\,mx} \geq 0.846\,T_x \tag{50}$$

which is smaller than the torque capacity Eqs. (24) or (27) for the four-wheel configurations. The power consumption for equal T_x, T_y, T_z is governed by the two indices presented in Table 2, and they indiate that the power consumed by the six-wheel configuration increases less rapidly than that by the four-wheel configurations.

The one-wheel-failure analysis, conducted earlier for the four-wheel configurations, is now, unfortunately, unwieldy because of the 5 × 3 size of six reduced transformation matrices. Therefore, pertinent results such as the torque capacity and the power consumption are obtained numerically and summarized in Table 2. Also, see Ref. 8 for one-cant angle, six-wheel configuration analysis.

Three-Wheel Pyramid Configuration

When wheel redundancy is not warranted, when for the reasons of cost and weight the number of wheels must be bare minimum, and when the torque requirements about the three axes are not necessarily equal, a three-wheel pyramid configuration is an ideal choice. Its cant angle optimization and sizing of the momentum and torque capacity of the wheels are dealt with in detail in Ref. 8; for its comparison with four- and six-wheel configurations, see Fig. 8 and Table 2.

Overall Comparison of Six Configurations

When the torque requirements about the roll, pitch, and yaw axes are not the same, the wheels of different torque capacities along each axis could be selected; but from the standpoint of reliability and cost that may not be preferred. A more attractive choice may be a six-wheel configuration with identical wheels, the cant angle of which is selected according to the desired torque ratios. For equal torque requirements, the optimum cant angle measured from the roll/yaw plane is $\eta^* = 35.26$ deg, and the associated wheel torque capacity for the required torque T_{mx} must be at least $0.846T_{mx}$ [Eq. (50)]—greater than $0.5T_{mx}$ for the two-wheel-per-axis orthogonal arrangement. The two power consumption indices, with no-wheel failure, are shown in the second row of Table 2. When one wheel fails, the torque capacity of the remaining five wheels must be raised to at least $1.311T_{mx}$ to produce the required torque T_{mx} about each spacecraft axis. This result is obtained by failing the wheels 1,2 . . . , 6, one at a time, and then determining the absolute maximum value of the wheel torque in each case to generate the torque T_{mx} about each axis. The maximum Euclidean norm and the associated absolute sum $\Sigma_{i=1}^{6}\,|\dot{H}_{wi}|$ are also shown in Table 2. Comparing the two-wheel-per-axis and the six-wheel hexagon configurations, we find that for equal torque requirement, the hexagon configuration requires the wheels of larger torque capacity and consumes more power, than and therefore is not as favored as the former configuration. However, when the roll, pitch, and yaw torque requirements are not the same

Table 2 Comparison of six configurations for equal torque about each spacecraft axis, for minimum power consumption

Required Control Torque: $T_X = T_y = T_z = T_{mx}$

Configuration	Optimum angle η^*, deg	No failure: Required torque capacity, $\dot{H}_{w,mx}/T_{mx}$	No failure: Total power consumption rate, $\Sigma_{i=1}^{n_w}\dot{H}_{wi}^2/T_{mx}^2$	No failure: Total power intercept due to nonzero initial wheel speed, $\Sigma_{i=1}^{n_w}\lvert\dot{H}_{wi}\rvert/T_{mx}$	Worst one-wheel failure: Required torque capacity, $\dot{H}_{w,mx}/T_{mx}$	Worst one-wheel failure: Total power consumption rate, $\Sigma_{i=1}^{n_w-1}\dot{H}_{wi}^2/T_{mx}^2$	Worst one-wheel failure: Total power intercept due to nonzero initial wheel speed, $\Sigma_{i=1}^{n_w-1}\lvert\dot{H}_{wi}\rvert/T_{mx}$
Two wheels/axis ($n_w = 6$)		0.5	1.5	3.0	1.0	2.0	3
Six-wheel hexagon ($n_w = 6$)	35.26	0.846	1.5	2.509	1.311	2.933	3.073
Four-wheel pyramid, base edges parallel to spacecraft axes ($n_w = 4$)	35.26	1.045	2.25	2.449	2.091	6.62	4.182
Four-wheel pyramid, base edges at 45 deg to roll and yaw axes ($n_w = 4$)	35.26	1.3	2.25	2.598	1.732	9.0	5.196
Three-wheel pyramid ($n_w = 3$)	35.26	1.39	3.0	2.8		Failure disallowed	
Three-orthogonal wheels ($n_w = 3$)		1	3.0	3.0			

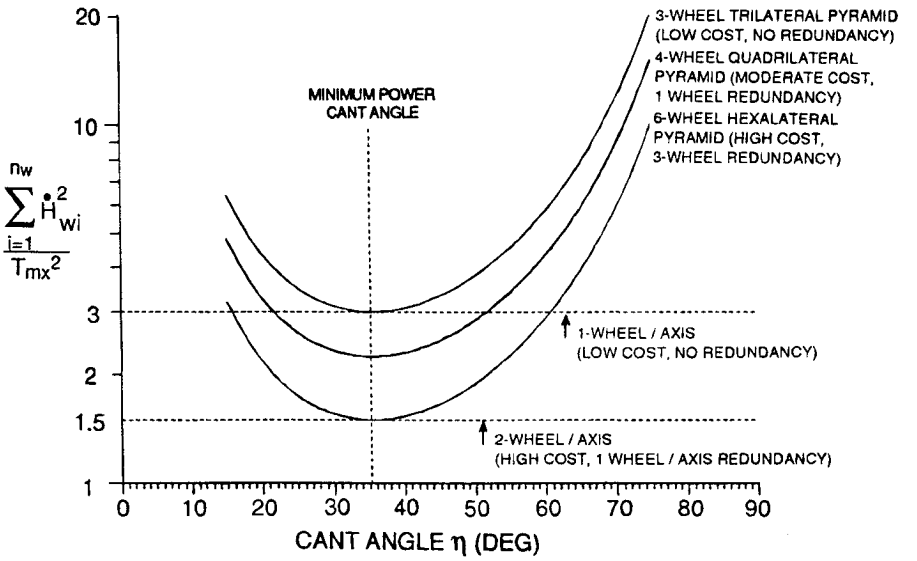

Fig. 8 Reaction wheel configurations tradeoffs for equal roll, pitch, and yaw torque requirements.

or when two wheels fail, the conclusion swings in favor of the hexagon configuration.

Although the six-wheel configurations provide substantial reliability and three-wheel redundancy, they are expensive, and so four-wheel configurations are desirable instead, providing only a one-wheel redundancy. Three such configurations, one with pyramid base parallel to the roll-yaw axes ($\gamma = 0$ deg), the second with the base at $\gamma = 45$ deg, and the third with a general γ, were discussed earlier. Under the no-failure case, the 45-deg configuration requires the wheels of larger torque capacity than the 0-deg configuration, but in the event of a one-wheel failure, the situation reverses (see Table 2). On the other hand, from the viewpoint of power consumption, under the no-failure case, the 45-deg configuration uses only slightly more power than the 0-deg configuration for a nonzero initial wheel speed, but the failure of a wheel aggravates this difference. Because the final design is usually based on the one-wheel-failure performance, we infer that if the power is relatively abundant and the wheel torque capacity is at a premium, the 45-deg configuration should be selected. On the other hand, if the power is expensive, then the 0-deg configuration is a prudent choice. The third four-wheel configuration (with a general γ) is eminently suitable when the roll/pitch/yaw torque requirements are not equal.

When wheel redundancy is not warranted, only three wheels—necessary and sufficient for spacecraft control—can be employed. If the torque and momentum requirements about the three axes are identical, the control engineer can opt for the one-wheel-per-axis configuration. But in the case of dissimilar requirements, a three-wheel pyramid, with the cant angle suitable to the desired torque and momentum ratios, is preferred. Table 2 compares these two three-wheel configurations for equal torque requirement (see the last two rows), and shows that the pyramid configuration requires wheels of 39% larger torque capacity; also its power consumption may be equal to or slightly less than that of the one-wheel-per-axis configuration, depending on the initial wheel speed.

Figure 8 sums up the comparison between the power consumption of the six configurations considered in Table 2 for equal torque requirement. In particular, the Euclidean norm of the vector $\dot{\boldsymbol{H}}_{ww}$ vs the cant angle for each configuration for the no-wheel-failure case are shown in the figure. As noted before,

the cant angle η^* ($\eta^* = 35.26$ deg) for minimum power consumption is the same for three-, four-, or six-wheel pyramid configurations.

V. Concluding Remarks

The sun-tracking commands developed here for both northern and southern arrays can be used in a number of ways. For a solar array articulated to the spacecraft at a fixed angle with the orbit plane, they can be used to determine this fixed angle for minimum average power loss, and to determine if, and how often, the 180-deg yaw rotations of the spacecraft are required over a year to minimize the power loss and maintain thermal equilibrium. On the other hand, for a solar array with two rotational degrees of freedom, these commands specify the arrays' instantaneous orientation relative to the spacecraft and, therefore, they can be used to evaluate the instantaneous vehicle inertia dyadic, gravity gradient torque arising from the products of inertia, atmospheric and solar radiation torque, and associated momentum accumulation both over an orbit and over one year. When this momentum is stored in the reaction wheels, they must be configured such that, for the required torque and momentum capacities about each spacecraft axis, their speed remains the lowest so as to minimize their power consumption. The optimum cant angles of the wheel pyramids, presented in the paper, serve that purpose. Additional relationships are presented for torque and momentum sizing of the reaction wheels in three-, four-, or six-wheel pyramid configurations.

Acknowledgments

With great pleasure, I acknowledge my indebtedness to my colleague Janis Indrikis, Flight Mechanics Group, for insightful technical discussion and for providing Fig. 3 and Eq. (7) in the paper. Also, I am grateful to Carl Hubert, Associate Editor, Martin Marietta Astro Space, Princeton, and to the reviewers of an earlier version of this paper for their helpful, thorough, and constructive reviews.

References

[1] McElvain, R. J., "Effect of Solar Radiation Pressure on Satellite Attitude Control," Proceedings of the American Rocket Society Guidance, Control, and Navigation Conference (Stanford, CA), Aug. 1961; also *Guidance and Control*, Progress in Astronautics and Rocketry, Vol. 8, edited by R. E. Roberson and J. S. Farrior, AIAA, New York, 1962, pp. 543–564.

[2] Dennehy, C. J., Kia, T., and Welch, R. V., "Attitude Determination and Control Subsystem for the TOPEX Satellite," *Proceedings of the AIAA Guidance, Navigation, and Control Conference* (Minneapolis, MN), Vol. 2, Aug. 1988, pp. 655–665.

[3] Kalweit, C. C., "Optimum Yaw Motion for Satellites with a Nadir-Pointing Payload," *Journal of Guidance, Control, and Dynamics*, Vol. 6, No. 1, 1983, pp. 47–52.

[4] DeBra, D. B., and Cannon, R. H., "Momentum Vector Considerations in Wheel-Jet Satellite Control System Design," *Guidance and Control*, Progress in Astronautics and Rocketry, Vol. 8, edited by R. E. Roberson and J. S. Farrior, AIAA, New York, 1962, pp. 565–598.

[5] Cannon, R. H., "Some Basic Response Relations for Reaction Wheel Attitude Control," *ARS Journal*, Jan. 1962, pp. 61–74.

[6] Fleming, A. W., and Ramos, A., "Precision Three-Axis Attitude Control Via Skewed Reaction Wheel Momentum Management," *Proceedings of the AIAA Guidance Navigation and Control Conference* (Boulder, CO), Aug. 1979, pp. 177–190.

[7] Kral, K., "Reaction Wheel Optimum Geometry," Sperry Flight Systems (now Honeywell), Phoenix, AZ, Dept. File 5240, Oct. 1986, p. 12.

[8] Hablani, H. B., "Momentum Accumulation Due to Solar Radiation Torque, and Reaction Wheel Sizing, with Configuration Optimization," *Proceedings of the NASA/Goddard Flight Mechanics/Estimation Theory Symposium* (Greenbelt, MD), May 1992, pp. 3–22.

[9] Evans, W. J., "Aerodynamic and Radiation Disturbance Torques on Satellites Having Complex Geometry," *Torques and Attitude Sensing in Earth Satellites*, Academic Press, New York, 1964, pp. 83–98.

[10] McLoughlin, F. A., and Tung, F. C., "Momentum Unloading Techniques for the Gamma Ray Observatory," Guidance, Navigation, and Control Conference (Seattle, WA), AIAA Paper 84-1838, Aug. 1984.